# Spiral waves on a contractile tissue

L. Mesin[1] and D. Ambrosi[2] [a]

[1] Dipartimento di Elettronica, Politecnico di Torino, Corso Duca degli Abruzzi 24, 10129 Torino, Italy
[2] MOX-Dipartimento di Matematica, Politecnico di Milano, piazza Leonardo da Vinci 32, 20133 Milano, Italy

**Abstract.** In a healthy cardiac tissue, electric waves propagate in the form of a travelling pulse, from the apex to the base, and activate the contraction of the heart. Defects in the propagation can destabilize travelling fronts and originate possible new periodic solutions, as spiral waves. Spiral waves are quite stable, but the interplay between currents and strain can distort the periodic pattern, provided the coupling is strong enough. In this paper we investigate the stability of spiral waves on a contractile medium in a non–standard framework, in which the electrical potential dictates the active *strain* (not *stress*) of the muscle. The role of conducting and contracting fibers is included in the model and periodic boundary conditions are adopted. A correlation analysis allows to evaluate numerically the range of stability of the parameters for the spiral waves, depending on the strain of the contracted fibers and on the magnitude of the stretch activated current.

**PACS.** 87.19.Hh Cardiac dynamics 87.19.rj Contraction

## Introduction

The mathematical modeling of the cardiac activity involves a number of challenging questions, spanning different fields of classical physics: solid mechanics, fluid dynamics and electrical signalling on excitable media, just to mention some relevant ones. A strong coupling exists among these phenomena: they occur at the same spatial and time scales, and there is no way to exert an action on the system without that an equally important feedback arises. As an example, consider the fluid–solid interaction. The heart pumps the blood through the circulatory system, but there is no hope to predict the mechanical contraction of the cardiac walls without addressing (in some approximated way, at least) the related fluid dynamics problem. In particular, the continuity of the stress at the internal surface of the cardiac wall rewrites in the equation of the elasticity (fluid dynamics, respectively) as a boundary condition that mainly determines the flowfield (the strain, respectively). In this sense, solid mechanics, fluid dynamics and electric signal shall be strongly coupled in ultimate models of the cardiac system.

This paper focusses on the coupling between two main actors of cardiac dynamics: nonlinear elasticity and electric signalling. The interest here is in the modification of the electric pattern due to the electromechanical interaction. Namely, we address the stability of spiral waves on an excitable medium, an issue largely inspired by the work by Panfilov and coworkers [12–14]. The intimate coupling between voltage waves and solid mechanics manifests itself in two directions. The electric signal activates the transmembrane currents of cardiac cells, cardiomyocites contract and stretch the cardiac chamber (the left ventricle, say), thus ejecting the corresponding volume of blood in the circulatory system. On the other hand, the stretch of the soft biological tissue acts as a feedback on the electric field in two ways. The strain of the domain modifies the slope of the gradients of voltage, so that waves travel faster [2]; however, this geometrical effect is weak compared to the much more important Stretch Activated Current (SAC) occurring at the level of some specific ionic channels [10].

There is a big number of mathematical models [5] that address the dynamics of ionic channels driven by the transmembrane voltage. The difference between the models is basically in the number of ion species to be detailed, possibly leading to a big number of ordinary differential equations coupled with a reaction diffusion equation for the voltage. Some features of the phenomenon can be caught by simpler phenomenological models with a mathematical structure which is quite standard: the spatial dynamics is represented by a linear diffusion term equation while currents are accounted for in a source term that is typically cubic. When the mechanoelectric feedback is taken into account, a SAC is to be included in the balance of action potential.

Spiral waves are periodic stable solutions of reaction–diffusion systems [8]. Spirals do not occur in the normal functionality of the cardiac tissue and their possible appearance can dramatically affect the healthy work of the cardiac pump; however it is commonly thought that defects in the diffusivity of ions can start up spirals. In such a context, the defibrillation of the tissue is an external electric action that depolarizes sinchronously all the cells, a sort of reboot of the system which allows that a source of action potential to generate a new, functional, pulse. An alternative possible action to reorganize the electric signal in the heart is of mechanical type: transmembrane currents can be activated by the (macroscopic) strain of the channels. For example, SAC is supposed to play an essential role when a precordial thump is used to terminate a cardiac arrhythmia.

The role of SAC on the propagation of electric waves has been extensively studied by Panfilov and coworkers. Their main result is that a large enough SAC can move the center of the spiral out [13] or even destroy the periodicity of the signal, originating chaotic voltage dynamics (and, as a consequence, also chaotic mechanical dynamics).

This paper proceeds in the same direction, using a mathematical model that differs in few aspects from their previous work.

- The mathematical model is simpler, as it does not include the known delay between voltage wave and contraction.
- The electromechanical coupling is addressed in the active strain framework, an approach that might have some mathematical advantages, as discussed in the paper.
- Periodic boundary conditions are adopted.
- Fibers are included in the diffusion of potential and in the elasticity of the quasi–incompressible tissue.

The last three points (coupling methodology, periodic conditions and anisotropy due to muscle fiber) are, in our opinion, steps more towards realistic bio–physical simulations.

The paper is organized as follows. Sections 1, 2 and 3 illustrate the mathematical model. Sections 4 is devoted to the bidimensional system of equations and to the numerical method we adopt. Section 4 collects the numerical results and their discussion.

# 1 Mechanics

We consider the heart as a hyperelastic body subject to external loads and active deformation that originate a strain field. Every material point is labelled by its own position at time $t = 0$. The motion of the point $\mathbf{X}$ at time $t$ is therefore defined by the vectorial map $\mathbf{x} = \mathbf{x}(\mathbf{X}, t)$ from the initial (relaxed) configuration to the current one. The gradient of this function is a tensor (the tensor gradient of deformation) indicated as follows:

$$\mathbf{F} = \operatorname{Grad} \mathbf{x}, \qquad F_{ij} = \frac{\partial x_i}{\partial X_j}, \qquad 1 \leq i, j \leq 3. \tag{1}$$

Here and in the following the symbols Grad and Div denote the gradient and the divergence operators, respectively, operated with respect to the $\mathbf{X}$ coordinates.
Following [6] we decompose the tensor gradient of deformation into two factors, the micro (active, $\mathbf{F}_o$) and the macro (passive, $\mathbf{F}_e$) one:

$$\mathbf{F} = \mathbf{F}_e \mathbf{F}_o. \tag{2}$$

The rationale of this decomposition is the following: fibers inside the muscle contract and become shorter. They form a kind of a watermark, defined in every point of the body, and the kinematics of this microstructure is resumed by $\mathbf{F}_o$, a distortion that does not preserve compatibility of the body, but dictates the deformation at a fiber scale. The deformation at the macroscale is measured by $\mathbf{F}_e$, that accounts both for the deformation of the material needed to ensure compatibility (possibly undermined by $\mathbf{F}_o$) and for the possible tension due to external loads. Notice that, in general, neither $\mathbf{F}_e$ nor $\mathbf{F}_o$ are gradients (they are not integrable) or, in other words, it does not exist any real motion that corresponds to fibers elongation without muscle contraction: indeed (2) is a pure theoretical decoupling that associates the microscale dynamics to the macroscale continuum mechanics.
We accordingly assume that the strain energy of the cardiac muscle depends only on the deformation at the macroscale

$$W = W(\mathbf{F}_e). \tag{3}$$

The electric potential travels across the muscle body, in a time-scale of the order of a few tenths of a second; this propagation mainly occurs along the preferential direction dictated by the orientation of the fibers, the same ones that primarily drive the mechanical contraction. However, the potential also diffuses normally to the fibers, the transverse conductivity being about one fourth of the longitudinal one [16]; the ratio of the velocities of propagation in the two directions is therefore of the order of two.
In a simple setting, one can assume that in any point $\mathbf{X}$ the fibers are oriented according to one direction only, namely

**n**. The unitary vector field $\mathbf{n}(\mathbf{X})$ denotes the (unique) direction of the fibers in $\mathbf{X}$ in the reference configuration of the body. The microscale part of the deformation tensor can take the simple form

$$\mathbf{F}_o = \mathbf{1} + \gamma(v)\mathbf{n} \otimes \mathbf{n}, \tag{4}$$

where $v$ is the electric potential and $\gamma$ is the activation function, to be constitutively prescribed. For a non–zero potential, it must be that $\gamma < 0$, denoting contraction. Note that $J_o = \det(\mathbf{F}_0) = 1 + \gamma$.

The Piola stress tensor $\tilde{\mathbf{P}}$ in the locally *intermediate configuration* is obtained by Frechet derivative of the strain energy (3)

$$\tilde{\mathbf{P}} = \frac{\partial W}{\partial \mathbf{F}_e}, \tag{5}$$

and it accounts for the tension due to the deformation $\mathbf{F}_e = \mathbf{F}\mathbf{F}_o^{-1}$. The corresponding force balance equation is conveniently written in the original reference configuration (spanned by the $\mathbf{X}$ coordinates) by a pull-back (see, for instance, [11]):

$$\text{Div}\left(J_o\tilde{\mathbf{P}}\mathbf{F}_o^{-T}\right) = 0, \tag{6}$$

to be supplemented by suitable boundary conditions.

Summarizing, the present model for the mechanics of the cardiac activity requires, from a constitutive viewpoint, a strain energy $W(\mathbf{F}_e)$, a geometrical description of the fiber vector field $\mathbf{n}(\mathbf{X})$ and a constitutive law for the activation function $\gamma(v)$ relating the electric potential $v$ to the fiber contraction.

The most popular alternative to the introduction of the decomposition sketched above is to include a new, addictive, active stress term in the force balance. This approach does not yield algebraic complications in the equations that characterize the active strain method. As a non–minor practical consequence, standard finite elements codes for finite elasticity cannot be easily adopted, because the active strain acts at an inner level in the equations. Conversely, an additive active stress can be simply included in standard codes and this may be one of the reasons that make this approach more popular.

In principle, at least, the active strain approach is more satisfactory from the modelling point of view, when the contraction of the observable fibers are included in the equations, while the active stress needs to be tuned in order that it can provide the observed deformation.

## 2 Electric activity

The propagation of the electrical signal in the cardiac muscle is determined by the ionic fluxes generated by a depolarization of the transmembrane potential. A broad literature exists on the modeling aspects of this process; the classical book by Keener and Sneyd [9] is an excellent introduction in this respect. However, as the focus of this work is on the electromechanical coupling, we restrict to a simple model that provides a correct qualitative dynamics for the propagation of the electric signal in a fixed domain, wherein the electric potential $v$ satisfies a diffusion–reaction equation coupled with a reaction–transport equation for the recovery variable $w$ (the Aliev–Panfilov model [1]):

$$\frac{\partial v}{\partial t} + \nabla \cdot (\dot{\mathbf{x}}v) - \nabla \cdot (\mathbf{D}\nabla v) = -kv(v - \alpha_1)(v - 1) - wv - I_{SAC}(v), \tag{7}$$

$$\frac{\partial w}{\partial t} + \nabla \cdot (\dot{\mathbf{x}}w) = \left(\varepsilon + \frac{\mu_1 w}{\mu_2 + v}\right)(w - kv(v - \alpha_2 - 1)). \tag{8}$$

Here $\mathbf{D}$ is a second order positive definite diffusion tensor. The symbol $I_{SAC}(v)$ denotes the stretch activated current. The symbols $\nabla$ and $\nabla\cdot$ denote the gradient and divergence operator in $\mathbf{x}$ coordinates (fixed in space, usually called *spatial coordinates* or also *Eulerian coordinates*), respectively. Note that (7) is a balance equation for the potential, accounting for the dynamics between diffusion and transmembrane currents of ionic species, whereas equation (8) does not involve any spatial flow besides convection. The divergence term at the left hand side represents the convective transport due to the displacement of the material itself as it can be observed by using coordinates fixed in space. These terms disappear when the equations are rewritten in material coordinates.

In a material frame of reference, assuming incompressibility (see also the following section), these equations rewrite (see, for instance, [2])

$$\frac{\partial v}{\partial t} - \text{Div}\left(\mathbf{F}^{-1}\mathbf{D}\mathbf{F}^{-T}\text{Grad}\,v\right) = -kv(v - \alpha_1)(v - 1) - wv - I_{SAC}(v), \tag{9}$$

$$\frac{\partial w}{\partial t} = \left(\varepsilon + \frac{\mu_1 w}{\mu_2 + v}\right)(w - kv(v - \alpha_2 - 1)). \tag{10}$$

## 3 Constitutive assumptions

The constitutive assumptions in this paper are kept at a minimum degree of complexity and, in fact, the discussion of the section above remains unaltered when applied to a reaction term at the right hand side of equation (7) more complicated than a cubic polynomial (i.e. more complex ionic models). Following the same vein, we restrict to considering an isotropic neo–Hookean material

$$W = W(\mathbf{F}_e) = \frac{\mu}{2}\left(I - 3\right), \tag{11}$$

where I is the first invariant of the left Cauchy–Green tensor of $\mathbf{F}_e$:

$$I = \operatorname{tr}\left(\mathbf{F}_e^T \mathbf{F}_e\right) = \mathbf{F}_e \cdot \mathbf{F}_e, \tag{12}$$

It is often assumed that biological materials can only undergo isochoric motion under load. This assumption usually stems by observing that biological materials are essentially made of water. In the present framework a material is incompressible, if the visible deformation $\mathbf{F}$ satisfies the kinematic constraint $J = \det \mathbf{F} = 1$. In this respect our approach differs from Cherubini et al. who assume $\det \mathbf{F}_e = 1$ [6]. After introducing the pressure $p$, the Lagrange multiplier enforcing incompressibility, a pull-back to the initial fully relaxed configuration for a neo-Hookean material, using the relation (6), yields the following form of the Piola tensor

$$\mathbf{P} = J_o \frac{DW}{D\mathbf{F}_e}\mathbf{F}_o^{-T} - Jp\mathbf{F}_e^{-T}\mathbf{F}_o^{-T} = \mu J_o \mathbf{F}\mathbf{F}_o^{-1}\mathbf{F}_o^{-T} - p\mathbf{F}^{-T}, \tag{13}$$

For a polynomial strain energy like (11), the active stress and the active strain approach can be reconciled: the active strain energy can be rephrased as a standard energy plus an active contribution. In the specific case of neo–Hookean material, we get

$$\begin{aligned}\mathbf{P} &= \mu\mathbf{F}\left(\mathbf{1} + J_o\mathbf{F}_o^{-1}\mathbf{F}_o^{-T} - \mathbf{1}\right) - p\mathbf{F}^{-T} \\ &= \mu\mathbf{F} - p\mathbf{F}^{-T} + \mu\left(J_o\mathbf{F}_o^{-1}\mathbf{F}_o^{-T} - \mathbf{1}\right),\end{aligned} \tag{14}$$

where $\mathbf{1}$ is the identity tensor and the last term at the right hand side can be understood as active stress contribution. However, we remark that this interpretation is not general and, in particular, does not apply to exponential strain energies, that are quite common in biomechanics. It is also worth to emphasize that a representation in terms of active stress, as shown in (14), is directly provided by the kinematics at the microscale, represented by $\mathbf{F}_o$ and leaves no room for any further modelling after identification of a suitable $\mathbf{F}_o$.

The activation function $\gamma$ introduced in equation (4) dictates the contraction of the cardiac muscle depending on the value of the potential. This activation is actually driven by the concentration of Calcium ions and is sometimes accounted for complicated dependencies. In this work we restrict ourselves to consider activation of the contraction proportional to the potential field, according to the following simple rule:

$$\gamma = -\beta v. \tag{15}$$

As the normalized potential satisfying the Aliev–Panfilov model takes only values between 0 and 1, $\gamma$ is always lower (depolarization phase) or equal to zero (rest potential), with negative values indicating fiber contraction. We are aware that such a crude coupling cannot account for well known spatio–temporal dynamics, as the relaxation time of the mechanical contraction is much longer than the potential pulse; however we decide again not to include such a delay for the time being in our model to keep the minimum degree of complexity.

The SAC is modeled in equation (7) by a term that activates only in case of stretch [13]:

$$I_{SAC}(v) = \begin{cases} G_s(I_C - 1)\left(v - 1\right) & \text{if } I_C > 1, \\ 0 & \text{if } I_C \leq 1, \end{cases} \tag{16}$$

where $G_s$ is a positive constant and $I_C$ is a measure of the strain that vanishes for $\mathbf{F} = \mathbf{1}$. This additive term is linear in $v$ and provides no contribution when there is no stretch ($I_C = 1$) or the potential takes its maximum value ($v = 1$). The mathematical role of this source term is to displace the equilibrium points that appear at the right hand side of equation (9) (see Appendix 1). In this work we take an orthotropic measure of the strain defined as

$$I_C = \mathbf{Fn} \cdot \mathbf{Fn}. \tag{17}$$

Equations (6), (9) and (10), supplemented by the constitutive assumptions (4), (13), (15) and the incompressibility constraint, together with initial and boundary conditions form our three dimensional setting for the electromechanical

cardiac coupling. Summarizing, the three–dimensional model reads:

$$\frac{\partial v}{\partial t} - \text{Div}\left(\mathbf{F}^{-1}\mathbf{D}\mathbf{F}^{-T}\text{Grad}\, v\right) = -kv(v - \alpha_1)(v - 1) - wv - I_{SAC}(v), \tag{18}$$

$$\frac{\partial w}{\partial t} = \left(\varepsilon + \frac{\mu_1 w}{\mu_2 + v}\right)(w - kv(v - \alpha_2 - 1)), \tag{19}$$

$$\text{Div}\left(\mu J_o \mathbf{F}\mathbf{F}_o^{-1}\mathbf{F}_o^{-T} - p\mathbf{F}^{-T}\right) = 0, \tag{20}$$

$$J = 1, \tag{21}$$

to be supplemented by suitable initial and boundary conditions, which were chosen as periodic in this study.

A comparison between the equations above and the model by Panfilov et al. [13] may help to point out how mechanics is here handled in a different way and some physical and physiological mechanisms are neglected herein. The first difference has been already discussed in depth: the potential here dictates the active strain, not the stress. This methodology is mathematically safer: desirable mathematical properties of the stress tensor that are straightforwardly satisfied in an "active strain" setting, may not be satisfied in a "active stress" approach (see Appendix 2). The second difference is that in the system (18)–(21) there is neither delay nor difference in wavelength between the electric and the mechanical wave; this effect is physiologically well known and could be taken into account considering a viscoelastic behavior of the tissue. Alternatively, one could consider more sophisticated models and relate the active contraction to calcium concentration, which is known to be characterized by a slower dynamics than the overall electric potential (see e.g. [4]). On the other hand, there are two characteristics of the model that make it more physiologically attractive: fibers dictate the (preferential) direction of diffusion and the direction of the contraction field. Secondly, periodic boundary conditions apply. Assuming periodic boundary conditions on a square is equivalent to take the topology of a "flat" torus, that is of course far from a real cardiac geometry; moreover, at the septum between atrium and ventricle, nonexcitable (insulating) cells are located. However, restricting to possible choices in two dimensions, in our opinion periodic boundary conditions are a more physiological framework than other options.

## 4 Two–dimensional electro–mechanical coupling

In this section we specify the general model described above to a two dimensional geometry and we illustrate the numerical method to be applied for the numerical approximation of the solution, that is reported in the last section.

### 4.1 Two–dimensional model

In the numerical simulations, we assume that the muscle fibers are uniformly oriented along the direction of the $X$ axis, so that $\mathbf{n} = (1, 0)$ in equation (4). The tensors gradient of deformation rewrite

$$\mathbf{F} = \begin{pmatrix} \frac{\partial x}{\partial X} & \frac{\partial x}{\partial Y} \\ \frac{\partial y}{\partial X} & \frac{\partial y}{\partial Y} \end{pmatrix}, \qquad \mathbf{F}_o = \begin{pmatrix} 1 + \gamma & 0 \\ 0 & 1 \end{pmatrix}. \tag{22}$$

The diffusion tensor $\mathbf{D}$ is now diagonal

$$\mathbf{D} = \begin{bmatrix} D_{xx} & 0 \\ 0 & D_{yy} \end{bmatrix}, \tag{23}$$

with larger diffusion along the fiber direction ($D_{xx} > D_{yy}$). Straightforward computations yield the following system of equations for the electrical problem

$$v_t = \left((D_{xx}y_Y^2 + D_{yy}x_Y^2)v_X - (D_{xx}y_X y_Y + D_{yy}x_X x_Y)v_Y\right)_X \tag{24}$$
$$+ \left((D_{xx}y_X y_Y + D_{yy}x_X x_Y)v_X - (D_{xx}y_X^2 + D_{yy}x_X^2)v_Y\right)_X - kv(v - \alpha_1)(v - 1) - wv - I_{SAC}$$

$$w_t = \left(\varepsilon + \frac{\mu_1 w}{\mu_2 + v}\right)(w - kv(v - \alpha_2 - 1)) \tag{25}$$

where the symbols $(\cdot)_t$, $(\cdot)_X$ and $(\cdot)_Y$ denote the partial derivatives with respect to $t$, $X$ and $Y$, respectively. Incompressibility is not strictly fulfilled from a numerical point of view, but compressibility is penalized in the strain energy by a quadratic term:

$$W = \frac{\mu}{2}\left(\mathbf{F}_e \cdot \mathbf{F}_e - 2\right) + \frac{\alpha}{2}(\det \mathbf{F} - 1)^2 \tag{26}$$

where, typically, $\alpha \gg 1$. Thus, the momentum balance equation reads

$$\text{Div} \left( \mu J_o \mathbf{F} \mathbf{F}_o^{-1} \mathbf{F}_o^{-T} + \alpha J(J-1) \mathbf{F}^{-T} \right) = 0. \tag{27}$$

The following system of equations is obtained

$$\begin{cases} \mu \left( \dfrac{x_X}{1+\gamma} \right)_X + \mu((1+\gamma)x_Y)_Y + \alpha(J_o(J-1)y_Y)_X - \alpha(J_o(J-1)y_X)_Y = 0 \\[2mm] \mu \left( \dfrac{y_X}{1+\gamma} \right)_X + \mu((1+\gamma)y_Y)_Y - \alpha(J_o(J-1)x_Y)_X + \alpha(J_o(J-1)x_X)_Y = 0 \end{cases} \tag{28}$$

## 4.2 Numerical Implementation

The differential problem (27)–(28) is numerically addressed by a finite difference approximation, implemented in Matlab (version 7.8.0 - R2009a). Spatial derivatives are approximated by a centered second order scheme. The discretization in time leads to decouple the electrical and mechanical problems at each time step. An implicit approximation in time for the non linear reaction term only gives the following expression for the updated potential field:

$$v^{n+1} = \frac{v^n + \Delta t \left( \text{Div}_d \left( J^n (\mathbf{F}^n)^{-1} \mathbf{D} (\mathbf{F}^n)^{-T} \text{Grad}_d \, v^n \right) - v^n w^n - I_{SAC}(v^n) \right)}{1 + \Delta t k \left( v^n - \alpha \right) \left( v^n - 1 \right)} \tag{29}$$

where $\text{Grad}_d$ and $\text{Div}_d$ indicate the discrete versions of the gradient and divergence operators, respectively, and $\Delta t$ is the time step. The ordinary differential equation for the recovery variable is implicit in the reaction term; using the updated potential provided by (29) the following algebraic expression is obtained

$$w^{n+1} = w_n + \Delta t \left( \varepsilon + \frac{\mu_1 w_{n+1}}{\mu_2 + v^{n+1}} \right) \left( w^{n+1} - k v^{n+1}(v^{n+1} - \alpha_2 - 1) \right) \tag{30}$$

The updated recovery variable is the unique positive solution of such an equation.
Expressing the activation function in terms of the updated potential, the mechanical problem (28) can be linearized and solved iteratively:

$$\begin{cases} \mu \left( \dfrac{x_X^{n+1}}{1+\gamma(v^{n+1})} \right)_X + \mu \left( (1+\gamma(v^{n+1}))x_Y^{n+1} \right)_Y + \alpha \left( J_o^n(J^n-1)y_Y^{n+1} \right)_X + \alpha \left( J_o^n(J^n-1)y_X^{n+1} \right)_Y = 0 \\[3mm] \mu \left( \dfrac{y_X^{n+1}}{1+\gamma(v^{n+1})} \right)_X + \mu \left( (1+\gamma(v^{n+1}))y_Y^{n+1} \right)_Y - \alpha \left( J_o^n(J^n-1)x_Y^{n+1} \right)_X - \alpha \left( J_o^n(J^n-1)x_X^{n+1} \right)_Y = 0 \end{cases} \tag{31}$$

## 4.3 Numerical Simulations

The discretized problem (31) now reads as a linear system, here solved using the Gaussian elimination Matlab routine optimized for sparse matrices.

The spatial domain is a square, the independent variable $X$ and $Y$ are between $-100$ and $100$ arbitrary units. We notice that different temporal and spatial scales characterize the potential and the mechanical problem. The potential undergoes stronger variations in time and space, so that a finer the temporal and spatial sampling is convenient for the electrical problem with respect to the mechanical one. We therefore adopt different integration steps for the two variables. The time step is $\Delta t = 1/50$ for the electrical problem and $t_{mech} = 50\Delta t = 1$ for the mechanical one. The spatial step is equal to 1 for the electrical problem and 4 for the mechanical one.

The penalization method adopted to enforce incompressibility (26) is dictated by the sake of simplicity: exact fulfillment of the incompressibility constrain involves a number of numerical difficulties that we do not want to address. However, a posteriori we have to control how distant is the solution from the constrain $J = 1$. The greatest discrepancy occurs when $\beta = 0.2$ and $G_s = 03$. In such a case, the maximum value of $|J - 1|$ in the computational domain is between 0.05 and 0.1, depending on time and the average error is of the order of 1%. While aware that this issue could be improved, we think that this weak compressibility is acceptable for our purposes.

Initial conditions are set up running the code on a rigid tissue. The spiral wave is generated from a segment of excited tissue (length 80, thickness 4) with an adjacent, partly superimposed segment of refractory region (length 80, thickness 3, superimposition region with a thickness of 1). The wave starts curling from the segment's end points. The wave dynamics is periodic after a few rounds. The solution computed at $T = 600$ is taken as initial condition for all the simulations that follow.
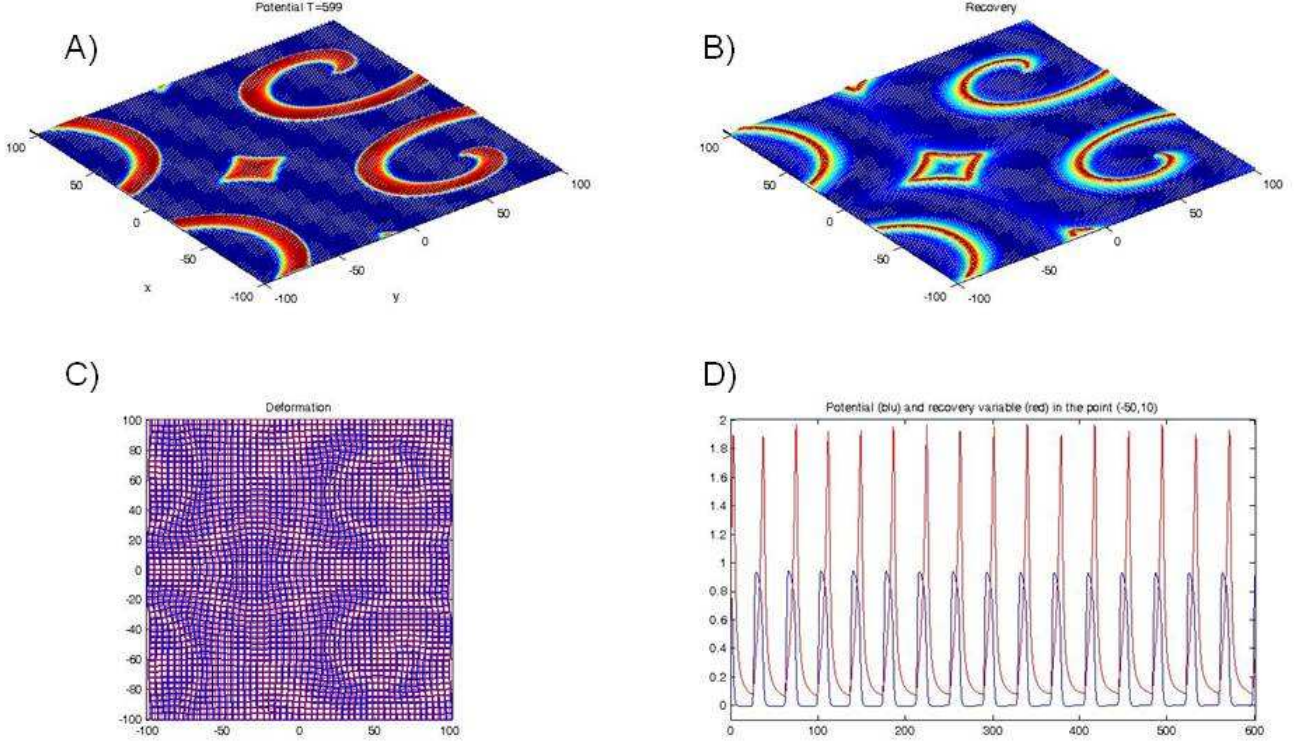
**Fig. 1.** Numerical simulation of spiral waves on a contractile medium with $\beta = 0.15$ and $G_s = 0.15$. Plots of the action potential (A) and of the recovery variable (B) at the final time. The relaxed and the deformed configuration (amplified times a factor 5, for graphical purposes) are compared in (C). Potential and recovery variable in a specific point of the domain are plot versus time in (D).

When the contractility of the medium is switched on, the electromechanical model simulates the dynamics of spiral waves in a deformable tissue. Relevant parameters to be tuned in our simulations are the contraction ratio $\beta$ and the conductance $G_s$ of the SAC: these parameters range between $5 - 45\%$ and $0 - 0.5$, respectively. The other parameters are fixed according to values taken from the literature [1], [16]: $k = 8$, $\alpha_1 = \alpha_2 = 0.15, \varepsilon = 0.002, \mu_1 = 0.2\,\mu_2 = 0.3\,\mu = 2000$, $D_{xx} = 2$, $D_{yy} = 1$, $\alpha = 600$. The numerical solution is computed till $T = 600$.

## 5 Results

Moderate values of contractility and SAC perturb slightly the system, and the dynamics of the spiral waves is not deeply modified by the electromechanical feedback. The results corresponding to the value of the parameters $\beta = 0.15$ and $G_s = 0.15$ are shown in Figure 1. The values of potential and recovery variable are mapped at the final time. The deformation of the tissue is shown in terms of relaxed and contracted position of the computational grid (amplified times a factor 5 for the sake of graphical evidence). The potential and the recovery variable for a specific point are plotted versus time: both fields are periodic functions of time (after a short transient). The only apparent role of the electromechanical coupling is a stretch of the potential in the direction of the fibers.

A quantitative indication of the influence of the strain of the tissue on the dynamics of the spiral waves can be provided by a two dimensional cross–correlation of the voltage field. As the electromechanical feedback modifies also the velocity of the action potential waves [2], a correlation between values of the electric field obtained with different parameters and evaluated at the same time would have no meaning. We therefore decide to correlate the voltage map
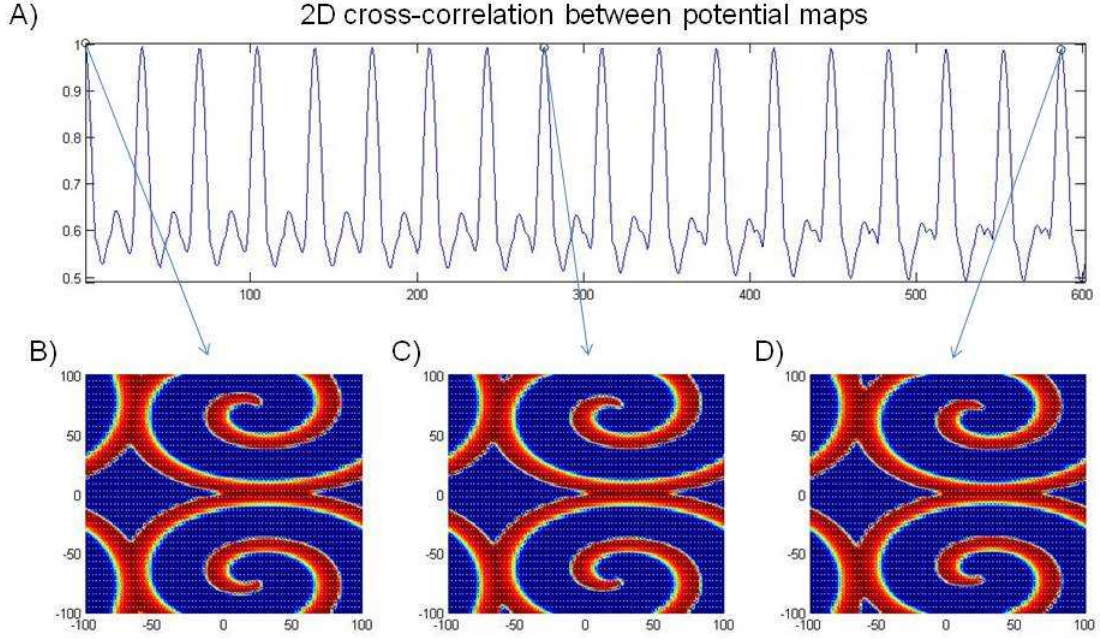
**Fig. 2.** Results of a numerical simulation with $\beta = 0.05$, $G_s = 0.05$. Two dimensional cross–correlation between potential maps (A). The color maps (B) - (C) - (D) represent the action potential field at three times, corresponding to local maxima of cross–correlation. The maximum of correlation is slightly less than one and the pattern is periodic: the spiral is very similar to the unstretched one and it is stable.

at time $t$ with the initial condition:

$$C(x, y, t) = \frac{\int \int v(X + x, Y + y, t = 0)\, v(X, Y, t)\, dX\, dY}{\sqrt{\int \int |v(X, Y, t = 0)|^2\, dX\, dY}\sqrt{\int \int |v(X, Y, t)|^2\, dX\, dY}}. \tag{32}$$

Possible rigid translations of the spiral are filtered out taking the maximum of the cross–correlation:

$$C_{\max}(t) = \max_{x,y} C(x, y, t). \tag{33}$$

This scalar function gives a quantitative indication of how much the map at time $t$ is similar to the initial conditions, corresponding to spiral waves on a rigid tissue. It is expected that maximum cross–correlation occurs when the spiral wave has undergone a period (a time interval possibly different from the "rigid" case). The value of $C_{\max}$ taken at that time gives a quantitative indication of the modification of the voltage field due to electromechanical effects. Exploiting the periodic boundary conditions we have adopted, the cross–correlation is computed in the Fourier domain. Figure 2 shows the maximum value of cross–correlation over the space variables as a function of time when $\beta = 0.05$, $G_s = 0.05$. The color maps represent the potential field at a given time, chosen at the peaks of correlation. For such low values of the relevant parameters, stable spirals persist.

For higher values of strain and SAC ($\beta = 0.15$ and $G_s = 0.15$) the cross–correlation remains periodic (figure 3), but the peak of correlation is lower: the signal remains periodic but the shape of the pattern is significantly different from the rigid one.

For higher values of strain and SAC, the periodicity of the cross–correlation is lost: the stability of the rigid case solution is lost and different scenarios arise. Figure 4 shows the solution for the case $\beta = 0.3$ and $G_s = 0.2$. Here correlation with the initial conditions is lost, but a new periodic wave appears.
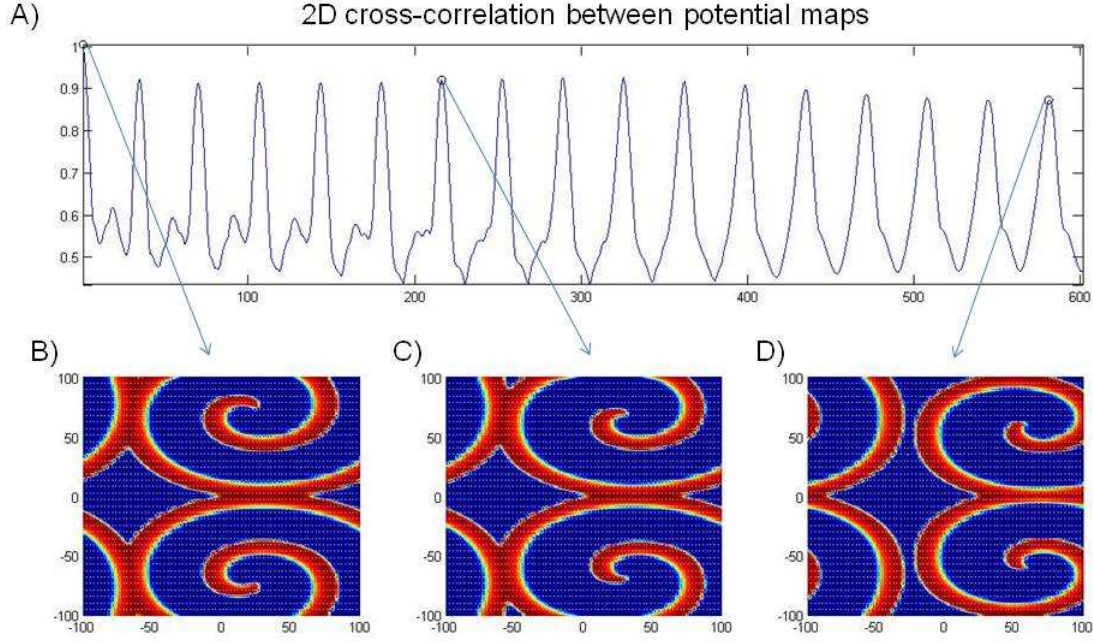
**Fig. 3.** Example of a numerical simulation for $\beta = 0.15$, $G_s = 0.15$. In this case the maximum of correlation with respect to the initial conditions is smoothly decreasing in time, but it preserves an oscillating behaviour with constant period. (A) Two dimensional cross–correlation between potential maps. (B) - (C) - (D) Potential maps at three times, corresponding to local maxima of cross–correlation.

When $\beta = 0.3$ and $G_s = 0.3$, patterns in the potential field can be still observed, but no periodicity is detected, at least according to our measure of correlation and in the time interval that we span with our simulations (Figure 5).

Finally, for high values of parameters, it sometimes happens that the potential extinguishes after a few oscillations (Figure 6). This is due to the interplay between the dynamics of the refractory regions (where the recovery variable is high) and the active regions (where potential is high). The active region is typically in front of the refractory one, but in the simulated finite periodic domain waves of potential can collide and the active strip can be erased by the refractory one. When the potential extinguishes within the first 500 time samples (corresponding to $10 - 12$ turns of the spiral), the solution is marked as *vanishing*. Some animations showing the dynamics of the potential maps are shown in the supporting material.

The variety of observed behaviors, depending on the strength of the biophysical forces, suggests to explore the plane of the parameters to obtain a synthetic information. In other words, we want to classify the stability of the spirals for given values of the $\beta$ and $G_s$ in terms of the maximal cross–correlation function (33). Figure 7 shows four quantities extracted from the cross–correlation, plotted in the $\beta$-$G_s$ plane:

– the trend of the peaks of cross–correlation (obtained by interpolating the peaks with a straight line),
– the mean period of spirals (computed as the mean time interval between two consecutive local maxima),
– the number of cycles in the time range considered (600 time units),
– the standard deviation of the period of the last spirals.

All these quantities are good indicators of the stability of our system: they are constant for stable spirals and they undergo an abrupt change for sufficiently large values of parameters. The observed qualitative behavior at the transition is as follows. At the onset of instability, the trend of peaks of cross–correlation starts decreasing, the mean period of spirals decreases (a smooth transition toward an unstable configuration or a different waveform) and the number of cycles decreases. At larger values of the parameters the cross–correlation shows an irregular behaviour: the trend of peaks of cross–correlation may be negative or positive (many irregularly spaced local maxima appear), a constant period cannot be identified any more and the number of cycles may decrease (leading to extinction of the spirals)
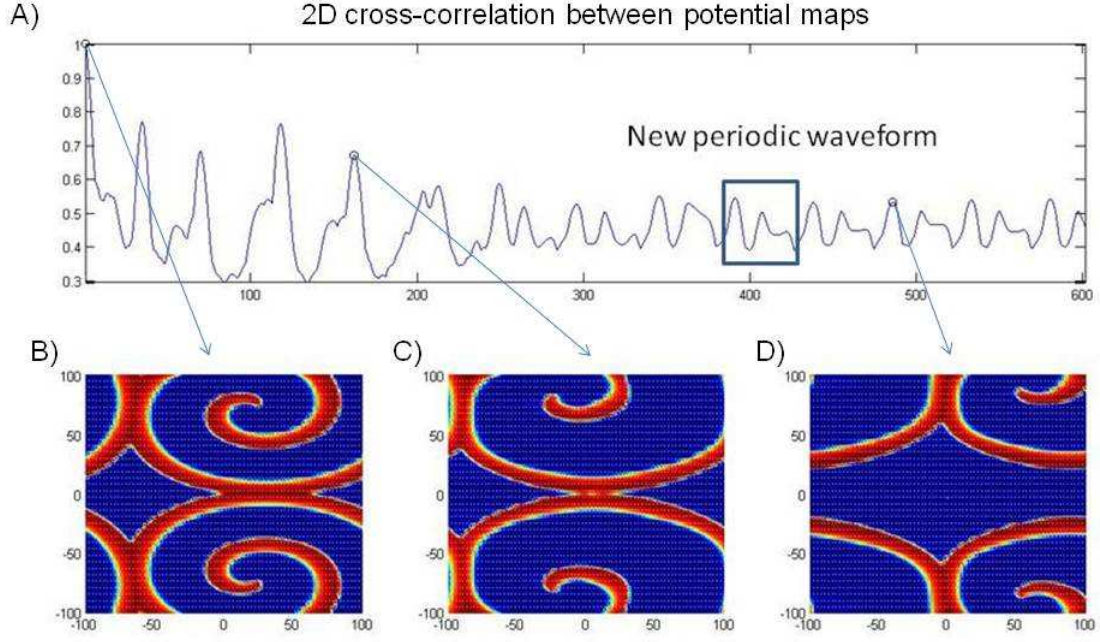
**Fig. 4.** Example of simulation with $\beta = 0.3$, $G_s = 0.2$. There is a periodic waveform different from the initial oscillations (indicated with a rectangle on the cross–correlation graph). (A) Two dimensional cross–correlation between potential maps. (B) - (C) - (D) Potential maps in three instants of time (corresponding to local maxima of cross–correlation).

or increase (erratic behaviour). Correspondingly, the standard deviation of the period increases (due to the irregular appearance of local maxima in the cross–correlation function).

A curve separating the stable and unstable regimes in the $\beta, G_s$ plane is tentatively plotted in Figure 7. Moreover, a red line is plotted to indicate the parameter values beyond which extinction of the spiral may occur (spirals are vanishing).

It is worth noticing that the complete extinction of the spiral does not deterministically happen when a threshold in the parameters is overcome: vanishing solutions are spotted in the unstable region of the $(\beta, G_s)$ plane. This suggests that the full extinction of a periodic nonlinear pattern in 2D with periodic boundary conditions is related to an interplay between the value of the parameters and the size of the domain: just when the length of the active and refractory regions and the size of the domain satisfy a suitable geometrical relation, the waves can fully superimpose and the signal vanishes.

## Concluding remarks

We have investigated the stability of spiral waves on a contractile tissue, where the electric signal dictates the mechanical contraction and the feedback is provided by a stretch activated current. The mathematical model is manifestly inspired by works on this subject appeared in the literature [13], with some relevant differences:

– the electromechanical coupling is addressed in the active strain framework,
– the biological tissue is quasi–incompressible,
– the material is in every point characterized by the fiber orientation **n**; this vector field has a role both in pointing the direction of faster diffusion of the potential and, more important, dictates the primary mechanical contraction,
– periodic boundary conditions apply.

All the listed differences are, in our opinion, improvements of the model towards its applicability to real biological systems and, in particular, cardiac mechanics.
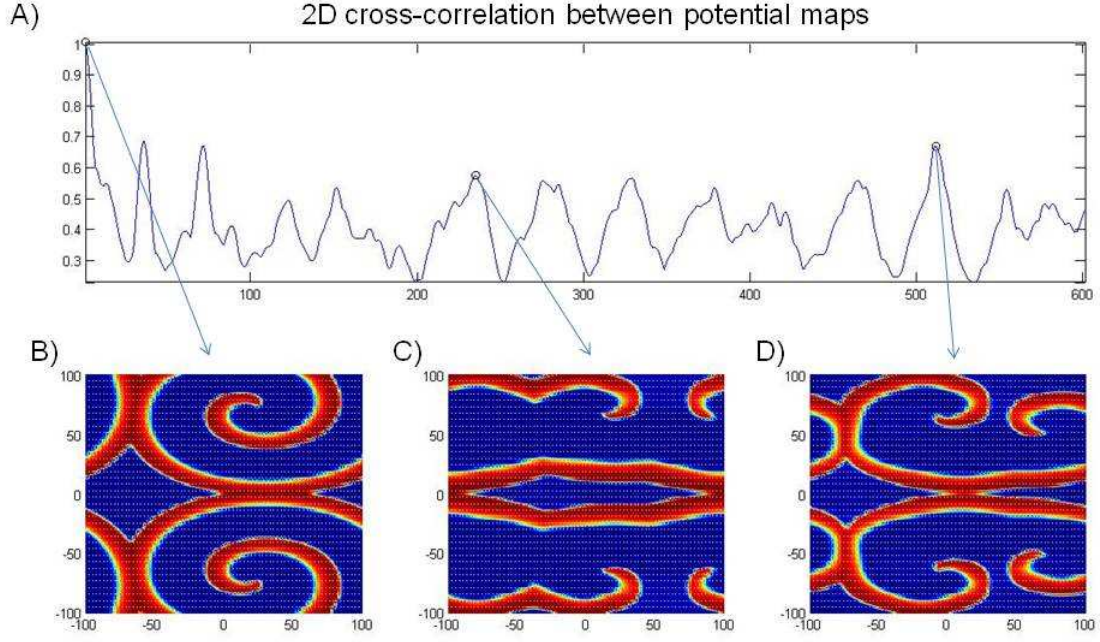
**Fig. 5.** Example of simulation with $\beta = 0.3$, $G_s = 0.3$. In this case the cross–correlation, after a few initial oscillations, appears to have a random behaviour. (A) Two dimensional cross–correlation between potential maps. (B) - (C) - (D) Potential maps in three instants of time (corresponding to local maxima of cross–correlation).

The two most relevant parameters for the dynamics of the system are $\beta$ and $G_s$, that tune the magnitude of the active strain and of the stretch activated current, respectively. We define the maximum cross–correlation between maps of voltage extracted at different times as the indicator of the stability of the spirals; the comparison is carried out with the solution of the electric wave on a rigid substrate. Exploring the plane of the $(\beta, G_s)$ parameters, we are able to distinguish the stable and unstable regions. The stable region corresponds to periodic solutions, detected by a periodic cross-correlation function: the period and shape of the spirals are different when different values of parameters are considered, but the same periodicity is preserved.

Unstable spirals occur when there is no periodic cross–correlation of the solution with the initial conditions. From the analysis of the dynamics of an unstable solution, different behaviors arise: onset of a new periodic solution, non–periodic travelling waves or signal extinction.

The numerical simulations of nonlinear problems, like the one at hand, suffer an intrinsic limitation: no extrapolation of the observed results for large time is applicable. As a matter of fact, when non–periodicity is observed in the time lapse of numerical simulations, we are not allowed to state that the signal is not periodic at all. However, in a biomedical perspective, the cardiac signal can have a random behavior just for a limited number of beats: the asymptotic behavior of the solution may be interesting from a speculative point of view, but it has a limited biomedical relevance.

In conclusion, the strength of the electromechanical coupling defines a stable/unstable transition for the dynamics of a spiral wave. According to our criteria and with the spatial resolution in the parametric plane that we have been able to use, a separation curve has been plotted. In the stable region, periodicity is preserved, with a maximum correlation that diminishes for bigger contractions and stretch activated currents. Beyond this region, the dynamics of the potential evolves toward a more complex behavior and eventually vanishes after a few turns.

## Appendix 1

Elementary calculations can provide the value of the parameters that determine the onset of self-excitatory behavior in the reaction–diffusion system. Appending a current source in equation (7) affects the zeroes of the cubic polynomial
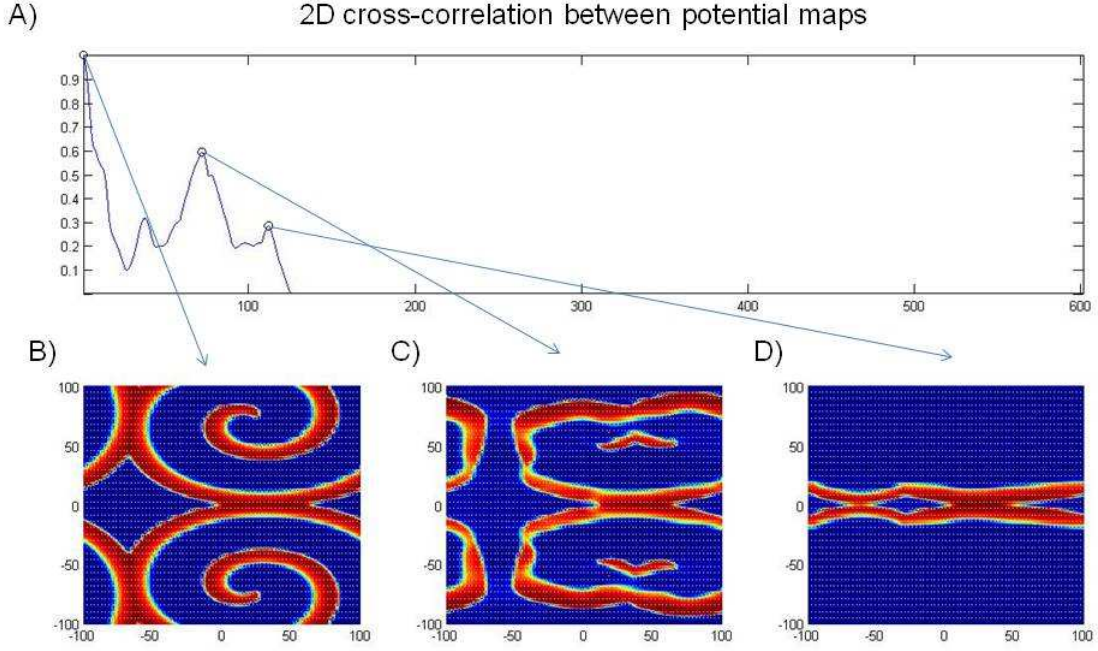
**Fig. 6.** Example of numerical simulation for $\beta = 0.3$, $G_s = 0.5$. In this case the correlation function and the potential field go to zero after a few oscillations. (A) Two dimensional cross–correlation between potential maps. (B) - (C) - (D) Potential maps in three times, corresponding to local maxima of cross–correlation.

in $v$ that appears at the right hand side. Consider the case of initially polarized cells ($v = w = 0$). For inert matter ($G_s = 0$), the three roots of the polynomial are $v = (0, \alpha_1, 1)$; the origin of the coordinates and $v = 1$ are stable equilibrium points, while $v = \alpha_1$ is unstable and no stretch can activate a current. When the SAC in the form (16) is added, $v = 1$ remains a stable equilibrium solution, while the other two roots become

$$v_\pm = \frac{\alpha_1}{2} \left( 1 \pm \sqrt{1 - \frac{4G_s(I_C - 1)}{\alpha_1 k}} \right). \tag{34}$$

Here $v_-$ is a stable equilibrium point while $v_+$ is unstable. As far as the value of $I_C$ is small, a finite step in potential (larger than $v_+ - v_-$) must be externally provided so that the system is destabilized and a polarization cycle can start. When $I_C$ increases, the two roots converge to the medium point $v = \alpha_1/2$. At the critical value

$$I_C - 1 = \frac{\alpha_1 k}{4G_s} \tag{35}$$

the two roots become imaginary and the dynamical system evolves in the direction of the only (stable) solution $v = 1$. In this configuration the system acts as a self-excitable one, although a relaxation of the strain recovers the original (non self-excitable) state.

A confirmation of these elementary arguments comes from the numerical results shown by Panfilov et al. [13]. Among other issues, these authors look numerically for the minimum value of the parameter $G_s$ to start up a pacemaker activity in a squared domain. For the value of the parameters adopted in that paper, $\alpha_1 = 0.05, k = 8, G_s = 0.5$, self-originated oscillations (i.e. instability of the configuration $v = 0$) should appear for $I_C - 1 = 0.25$: for such a value the voltage rapidly raises the value $v = 1$ and a cycle starts. That is exactly the numerical value reported by the authors in the plot of figure 4b in [13].
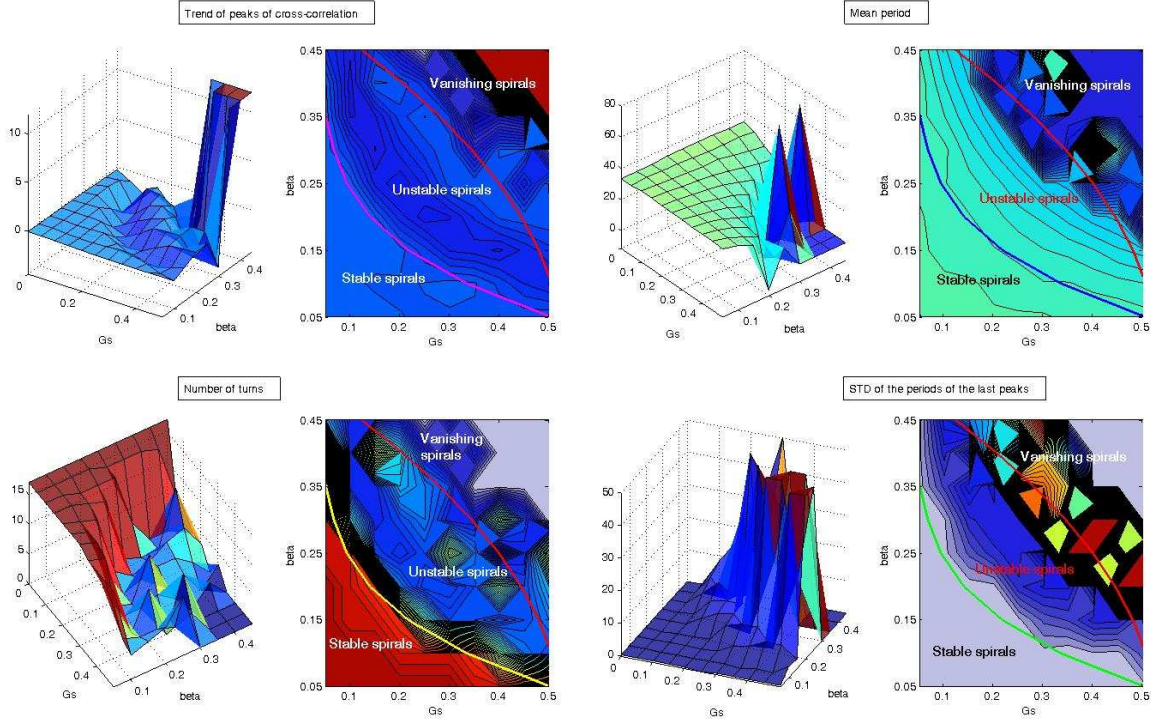
**Fig. 7.** Behaviour of four variables (trend of correlation, mean period of spirals, number of cycles in the time range considered, standard deviation of the period of the last 50% of spirals identified) extracted from the 2D cross–correlation of potential maps as a function of the parameters $\beta$ and $G_s$. The surface map is shown for each parameter on the left and a contour plot is shown on the right. A curve separating stable values of variables (indicating stable spirals) from a small variation (indicating the onset of instability) is also shown superimposed to the contour plot, together with a red line indicating the limit of parameters beyond which extinction of the spirals may occur.

## Appendix 2

In the active stress framework, the total Piola stress reads

$$\mathbf{P} = \frac{\partial W}{\partial \mathbf{F}} - p\mathbf{F}^{-T} + \mathbf{P}_a(\mathbf{F}). \tag{36}$$

It is commonly required that the minimum mathematical characterization for the constitutive relation defining a stress tensor is that it it must be strictly convex. Under sufficient regularity, this means

$$\mathbf{H} \cdot \frac{\partial \mathbf{P}}{\partial \mathbf{F}} \cdot \mathbf{H} > 0, \tag{37}$$

must hold for any any rank–one tensor $\mathbf{H}$ [3].
This requirement is sometimes neglected in active stress models. As an example consider

$$\mathbf{P}_a = \mu_2 \mathbf{F}^{-T}, \tag{38}$$

then

$$\mathbf{H} \cdot \frac{\partial \mathbf{P}}{\partial \mathbf{F}} \cdot \mathbf{H} = -\mu_2 \mathbf{F}^{-T} \mathbf{H}^T \mathbf{F}^{-1} \cdot \mathbf{H} < 0, \tag{39}$$

for any $\mathbf{H} = a \otimes a$.

## References

1. Aliev RR and Panfilov AV, A simple two-variable model of cardiac excitation, *Chaos, Solitons & Fractals*, 7: 293-301 (1996).

2.  Ambrosi D, Arioli G, Nobile F and Quarteroni A, Electromechanical coupling in cardiac dynamics: the active strain approach, submitted.
3.  Antman, S.S., *Nonlinear Problems in Elasticity*, Second edition, Springer (2005).
4.  Bers DM, Cardiac excitation-contraction coupling, *Nature*, 415:198–205 (2002).
5.  Bueno-Orovio A, Cherry EM and Fenton FH, Minimal model for human ventricular action potentials in tissue, *Journal of Theoretical Biology*, 253(3)–544-560 (2008).
6.  Cherubini C, Filippi S, Nardinocchi P and Teresi L, An electromechanical model of cardiac tissue: Constitutive issues and electrophysiological effects, *Progr. Biophys. Molec. Biol.*, 97:562-573 (2008).
7.  Cherubini C, Filippi S, Nardinocchi P and Teresi L, Electromechanical Modelling of Cardiac Tissue, in *Mechanosensitivity of the Heart*, 421-449 (2010).
8.  Fenton FH and Karma A, Vortex dynamics in three-dimensional continuous myocardium. Filament instability and fibrillation, *Chaos* 8:20-47 (1998).
9.  Keener J and Sneyd J, *Mathematical Physiology*, Springer (1998).
10. Kohl P, Hunter P and Noble D, Stretch-induced changes in heart rate and rhythm: clinical observations, experiments and mathematical models *Progress in Biophysics and Molecular Biology* 71(1):91-138 (1999)
11. I-Shih Liu, *Continuum Mechanics*, Springer (2002).
12. Nash MP and Panfilov AV, Electromechanical model of excitable tissue to study reentrant cardiac arrhythmias, *Progr. Biophys. Molec. Biol.*, 85:501522 (2004).
13. Panfilov AV, Keldermann RH and Nash MP, Self–organized pacemakers in a coupled reaction–diffusion–mechanics system, *Phys. Rev. Lett.*, 95:258104 (2005).
14. Panfilov AV, Keldermann RH and Nash MP, Drift and breakup of spiral waves in reaction-diffusion-mechanics-system *PNAS* 104:7922-7926 (2007).
15. Pathmanathan P, Chapman SJ, Gavaghan DJ and Whiteley JP, Cardiac Electromechanics: The Effect of Contraction Model on the Mathematical Problem and Accuracy of the Numerical Scheme, *Quarterly J. Mech. Appl. Maths.* 63(3):375–399 (2005).
16. Stinstra JG, Shome S, Hopenfeld B and MacLeod RS, Modelling passive cardiac conductivity during ischaemia, *Med Biol Eng Comput.* 43(6):776-82 (2005).